The formation and mitigation of nitrate pollution: Comparison between urban and suburban environments

Suxia Yang[1,2], Bin Yuan[1,2*], Yuwen Peng[1,2], Shan Huang[1,2], Wei Chen[3], Weiwei Hu[3], Chenglei Pei[3,4,5,6], Jun Zhou[1,2], David D. Parrish[1], Wenjie Wang[7], Xianjun He[1,2], Chunlei Cheng[2,8], Xiaobing Li[1,2], Xiaoyun Yang[1,2], Yu Song[8], Haichao Wang[9], Jipeng Qi[1,2], Baolin Wang[10], Chen Wang[10], Chaomin Wang[1,2], Zelong Wang[1,2], Tiange Li[1,2], E Zheng[1,2], Sihang Wang[1,2], Caihong Wu[1,2], Mingfu Cai[1,2], Chenshuo Ye[6], Wei Song[3], Peng Cheng[7], Duohong Chen[6], Xinming Wang[3], Zhanyi Zhang[1,2], Xuemei Wang[1,2], Junyu Zheng[1,2], Min Shao[1,2*]

[1]Institute for Environmental and Climate Research, Jinan University, Guangzhou 511443, China

[2]Guangdong-Hongkong-Macau Joint Laboratory of Collaborative Innovation for Environmental Quality, Jinan University, Guangzhou 511443, China

[3]State Key Laboratory of Organic Geochemistry and Guangdong Key Laboratory of Environmental Protection and Resources Utilization, Guangzhou Institute of Geochemistry, Chinese Academy of Sciences, Guangzhou 510640, China

[4]CAS Center for Excellence in Deep Earth Science, Guangzhou, 510640, China

[5]University of Chinese Academy of Sciences, Beijing 100049, China

[6]Guangzhou Ecological and Environmental Monitoring Center of Guangdong Province, Guangzhou 510060, China

[7]State Joint Key Laboratory of Environmental Simulation and Pollution Control, College of Environmental Sciences and Engineering, Peking University, Beijing 100871, China

[8]Institute of Mass Spectrometry and Atmospheric Environment, Guangdong Provincial Engineering Research Center for on-line Source Apportionment System of Air Pollution, Jinan University, Guangzhou 510632, China

[9]School of Atmospheric Sciences, Sun Yat-Sen University, Guangzhou 510275, China

[10]School of Environmental Science and Engineering, Qilu University of Technology, Jinan 250353, China

*Correspondence to: Bin Yuan (byuan@jnu.edu.cn) and Min Shao (mshao@pku.edu.cn)

Text S1. Split model configuration

During the observation periods, the diurnal variations of planetary boundary layer (PBL) at the GIG and Heshan sites are shown in Fig.S1 (a, b), which are based on data from the website of NOAA Air Resource Laboratory (https://ready.arl.noaa.gov/READYamet.php). The PBL height decreased significantly at 17:00, which would decouple into nocturnal surface boundary layer (NBL) and residual layer (RL). Besides, O_3 and NO_x at the ground site and 488 m site of Canton Tower agreed well during the day (shown in Fig. 5 (a) ~ (c)), and started to show clear distinction from 17:00, thus we define 17:00 as the sunset time. At that time, the box was initialized by the last condition of the daytime model, and was separated into NBL and RL boxes. As the average boundary layer height was 400 m and 1000 m in the nighttime and daytime respectively, the heights of NBL and RL were set to 400 m and 600 m (Fig.S1 (c)). Both nighttime boxes were simulated from 17:00 to the next morning 06:00, at which time the PBL height began to gradually increase. After 06:00, we assumed RL and NBL layer began to mix as the NBL height linearly increased, instantaneously mixing once per hour until 10:00, the mixing process was completed, and two boxes were combined as a whole box. The mixed layer height was set as 1000 m in the simulation of daytime from 10:00 to 17:00.

In the nighttime at the GIG site, the trace gases of NO_2 and O_3, meteorological parameters RH and *T* in the RL box, were constrained by the measurements from the 488 m site at Canton Tower. Several arguments justify this approach. Firstly, the trace gases at the surface GIG site were comparable with the Canton ground site in Fig.5, especially during the nighttime; the mean concentration deviations for NO, NO_2 and O_3 between the GIG and Canton ground sites were 1.96%, 6.54% and 0.65%, respectively. In addition, given the short distance between locations, we expect the composition of the aloft RL layer at GIG site to be closely represented by the Canton 488 m site. The O_3 at the Canton 488 m site was higher than at the ground site, and relatively unaffected by surface NO emissions, which would promote the nighttime NO_3 - N_2O_5 chemistry. The temporal evolution of other species in the RL, such as NO and VOCs, were unconstrained, and thus calculated by the box model.

However, there was no measurement aloft available for the campaign at Heshan site. Therefore, all species observed at Heshan site at 17:00 are set as the initial inputs for the RL box to freely evolve over night. To test this setting, we performed a simulation experiment using observations at GIG and Canton Tower sites. In analog to the settings of Heshan site, the observations at 17:00 at the GIG site were used as the initial inputs of RL, and allowed the initial data to freely evolve at night, without the influence from surface emissions. As shown in Fig.S6, the simulated nighttime results of NO_2 and NO_x in the RL compared well with the observation at the 488 m site of Canton Tower, which showed good agreements. Simulated O_3 and Ox were lower than the observations at the 488 m site of Canton Tower, but were within the combined uncertainties.

The physical loss that parameterized as a dilution process with a lifetime of 24 h was the same as the daytime simulation in both the NBL and RL. In addition to this loss, the dry deposition rate for HNO_3 and O_3 were treated as first-order loss reactions in the model, set as 2.7 and 0.42 cm s^{-1} in the daytime, 0.88 and 0.14 cm s^{-1} in the nighttime NBL, as the deposition rate is known to decrease after sunset (Zhang et al., 2003;Womack et al., 2019).

Text S2 Calculation of nitrate production

The different mechanisms that increased nitrate concentrations in the simulations included three contributions: the reaction of OH and NO_2, heterogenous N_2O_5 uptake to the ground in the NBL, and nitrate mixed to the ground from the RL in the morning. The first two contributions were calculated by Eq. S (1) and Eq. S (2), combined with the R1 and R5 listed in the main text, which represented the nitrate production rate in surface boundary layer. The OH, N_2O_5 were based on the model results. $k_{[OH][NO_2]}$ was from the website of MCMv3.3.1 (https://mcm.york.ac.uk/).

$$P_{OH+NO_2} = k_{[OH][NO_2]}[OH][NO_2] * F \quad \text{S(1)}$$

$$P_{NBL(N_2O_5\ uptake)} = \frac{\omega 1 * \gamma * Sa}{4}[N_2O_5](2-\varphi) * F \quad \text{S(2)}$$

The production rate of OH + NO_2 in the model is the total HNO_3 production rate. The heterogenous N_2O_5 uptake production rate in the NBL is based on S (2), here F

represents the partition ratio between HNO_3 and nitrate, which is calculated by Cp/ (Cp + Cg), where Cp and Cg are the observed concentration of nitrate and HNO_3, respectively.

With the convective growth of the planetary boundary layer (PBL) following sunrise, the polluted species in RL are vertically entrained into the NBL, which changes surface pollutant concentrations (Curci et al., 2015;Chen et al., 2020). We assume the entrainment mixing process occurred from 6:00 to 10:00 (shown in Fig.S1 (c)), when the height of PBL (H_{PBL}) increased from 400 m to 1000 m, on the contrary, the height of RL (H_{RL}) linearly decreased from 600 m to 0 m, the nitrate produced from NBL and RL would participate in this process. The instantaneous mixed nitrate concentration (C_{mixed}) was the sum of nitrate mixed from RL (C_{RL}) and NBL (C_{NBL}), and the nitrate enhancement from the mixing process (P_{mixed}) was calculated by the difference of mixed nitrate concentration and the NBL nitrate concentration (C_{NBL}), which was described as follows:

$$C_{mixed,i} = C_{RL,i} \times \frac{H_{RL,i-1} - H_{RL,i}}{H_{PBL,i}} + C_{NBL,i} \times \frac{H_{PBL,i-1}}{H_{PBL,i}} \quad \text{S (3)}$$

$$P_{mixed,i} = C_{mixed,i} - C_{NBL,i} \quad \text{S (4)}$$

here *i and i-1* represent the current and previous time step, the changing height of different layers represent the weight coefficient of mixed nitrate concentration in RL and NBL. The hourly surface nitrate production was the sum of P_{OH+NO2}, $P_{NBL(N_2O_5\ uptake)}$ and $P_{mixed,}$ the total nitrate production in one day included the integral production of P_{OH+NO2} in the daytime (7:00 to 17:00), $P_{NBL(N_2O_5\ uptake)}$ in the nighttime (from 17:00 to 6:00 in the next morning), and P_{mixed} from 6:00 to 10:00 in the morning.

Text S3 Sensitivity test of isopleth diagrams from F0AM box model simulations.

In addition to the discussions about model simulation, several parameters used in the box model might influence the simulation results, which include the concentrations of HONO, the N_2O_5 uptake coefficient (γ) and the $ClNO_2$ yield (φ) (Lammel and Cape, 1996). Due to the uncertainty of HONO source and limited measurements, previous studies used the ratio between HONO and NO_x to constrain HONO, such as 0.8% in

the high density traffic period in urban areas (Kurtenbach et al., 2001), 2% in the global chemical transport model (Elshorbany et al., 2012;Tan et al., 2019). In this study, we used the observed HONO as the base case, and ran the model in different sensitivity scenarios: with 0.8% of NO_x, with 2% of NO_x and with 2% of NO_2 as HONO concentrations (Fig. S8). Despite the different concentrations of HONO used in the simulation, they all showed similar variation patterns for ozone and nitrate, indicating little influence of the HONO concentration parameterization on the simulation results. The γ and φ changed widely between laboratory and field studies (Mozurkewich and Calvert, 1988;Riedel et al., 2014;Wang et al., 2017;Yun et al., 2018;McDuffie et al., 2018). The parameterized γ and φ by updated empirical method by Yu et al. (2020) was applied in the base model. As we only chose the median value of φ as the input parameter; thus, different values of φ were selected to perform sensitivity simulation (Fig. S9). Compared with the base case, the sensitivity of nitrate did not change with different values of φ, and the peak values of nitrate showed little difference. Overall, varying HONO and the $ClNO_2$ yield would not be expected to change the sensitivity region of ozone and nitrate.

Table S1. Measured chemical species and the analytical methods, time resolution, limit of detection and the accuracy of the instruments used for different measured species.

chemical species	methods	time resolution	limit of detection	accuracy
NMHC	GC-FID-MS	1 h	10 ~ 84 ppt	0.65% ~ 9.14%
Formaldehyde	PTR-TOF-MS	1 min	20 ppt	11.8%
Acetaldehyde	PTR-TOF-MS	1 min	33 ppt	12.5%
HNO_3	TOF-CIMS	1 min	< 10 ppt	± 20%
N_2O_5	TOF-CIMS	1 min	< 10 ppt	± 25%
$ClNO_2$	TOF-CIMS	1 min	< 10 ppt	± 25%
NH_3	CRDS	1 min	1.0 ppb	± 35%
NH_3	GAC	30 mins	0.08 ppb	_
HONO	LOPAP	1 min	6.0 ppt	± 20%
HONO	GAC	30 mins	0.1 ppb	_
O_3	UV absorption	1 min	0.5 ppb	± 10%
$NO/NO_2/NO_x$	Chemiluminescence	1 min	0.4 ppb	± 10%
CO	Infrared absorption	1 min	0.04 ppm	± 10%
NO_3^-, SO_4^{2-}, NH_4^+	TOF-AMS	300 s	0.005~0.024 μg m^{-3}	± 20%
Sa	APS, SMPS	300s	—	± 10%
Photolysis frequencies	Spectrometer	10 s	—	± 10%

Table S2. The mean volumetric concentrations of VOCs detected at the GIG and Heshan sites (Units: ppb)

Site	GIG	Heshan		GIG	Heshan
Species	Average ± SD		Species	Average ± SD	
Ethane	3.71±1.24	3.18±0.71	n-Heptane	0.11±0.15	0.24±0.23
Ethene	1.78±1.05	1.77±0.98	2-Methylheptane	0.02±0.02	0.13±0.2
Propane	6.88±5.1	4.22±1.85	3-Methylheptane	0.02±0.02	0.14±0.21
Propene	0.4±0.41	0.28±0.18	Toluene	2.02±1.9	3.44±1.65
i-Butane	1.76±1.32	1.64±0.8	n-Octane	0.05±0.05	0.25±0.18
n-Butane	3.15±2.46	3.17±1.67	Ethylbenzene	0.32±0.32	1.04±0.65
Acetylene	1.93±0.74	2.25±0.78	m/p-Xylene	0.91±0.87	4.01±2.22
trans-2-Butene	0.03±0.03	0±0.01	Nonane	0.04±0.03	0.24±0.07
1-Butene	0.08±0.05	0.05±0.04	o-Xylene	0.33±0.33	1.38±0.88
cis-2-Butene	0.02±0.02	_	Styrene	0.13±0.22	0.44±0.57
i-Pentane	1.33±1.06	2.38±2.6	Isopropylbenzene	0.01±0.01	0.1±0.1
n-Pentane	0.76±0.68	2.37±3.65	n-Propylbenzene	0.01±0.01	0.11±0.06
1-Pentene	0.03±0.02	0.01±0.01	m-Ethyltoluene	0.03±0.03	0.14±0.06
trans-2-Pentene	0.01±0.02	0±0.01	p-Ethyltoluene	0.02±0.02	0.15±0.07
Isoprene	0.14±0.15	0.14±0.19	n-Decane	0.02±0.02	0.06±0.02
cis-2-Pentene	0.01±0.01	0±0.01	1,3,5-Trimethylbenzene	0.02±0.02	0.13±0.04
2,2-Dimethylbutane	0.04±0.03	0.04±0.02	o-Ethyltoluene	0.02±0.01	0.1±0.03
2,3-Dimethylbutane	0.06±0.05	0.53±0.31	1,2,4-Trimethylbenzene	0.06±0.07	0.1±0.05
1-Hexene	0.02±0.01	0.02±0.06	1,2,3-Trimethylbenzene	0.02±0.01	0.06±0.02
n-Hexane	0.58±0.83	0.41±0.27	n-Undecane	0.01±0.01	_
2-Methylhexane	0.11±0.14	0.31±0.24	n-Dodecane	0.06±0.04	_
3-Methylhexane	0.13±0.18	0.32±0.25	Formaldehyde	2.53±1.62	2.42±1.2
Benzene	0.46±0.17	0.58±0.2	Acetaldehyde	1.95±1.2	3.14±1.64

146 **Table S3.** The concentrations of chemical components (average ± standard deviation)
147 and meteorological parameters during the investigated periods at the GIG and Heshan
148 sites
149

Site	GIG	Heshan
PM_1 (μg m^{-3})	41.7±23.1	40.6 ±15.5
Organic (μg m^{-3})	16.9±9.0	21.6 ± 9.0
SO_4^{2-} (μg m^{-3})	10.1±4.6	6.9 ± 1.8
NO_3^- (μg m^{-3})	6.1±5.8	3.9 ± 3.0
NH_4^+ (μg m^{-3})	5.0±3.0	3.5 ± 1.5
Cl^- (μg m^{-3})	0.6±0.54	0.8 ± 1.3
BC (μg m^{-3})	3.2±1.1	4.0 ± 1.6
WS (m/s)	1.9±0.9	1.6±0.7
RH (%)	76.2±14.9	59.5±14.3
T(°C)	23.0±2.6	23.2±3.2

150
151

Table S4. Model performance for nitrate at GIG and Heshan sites

Site	Species	Observed	Modeled	MB[a]	RMSE[b]	IOA[c]	r[d]
GIG	Nitrate ($\mu g\ m^{-3}$)	6.2	7.4	1.2	4.9	0.84	0.77
Heshan	Nitrate ($\mu g\ m^{-3}$)	3.9	3.91	0.12	1.4	0.71	0.59

[a]: mean bias (MB), here we define the Obs_i and Mod_i as the observed and modeled values at time i, respectively, and N represents the number of observations.

$$\mathrm{MB} = \frac{\sum(Mod_i - Obs_i)}{N}$$

[b]: root mean square error (RMSE);

$$\mathrm{RMSE} = \sqrt{\frac{1}{N}\left(\sum_{i=1}^{N}(Mod_i - Obs_i)^2\right)}$$

[c]: index of agreement (IOA), Obs_{aver} and Mod_{aver} represent the average concentration of observation and model, respectively.

$$\mathrm{IOA} = 1 - \frac{\sum_{i=1}^{N}(Obs_i - Mod_i)^2}{\sum_{i=1}^{N}(|Obs_i - Obs_{aver}| + |Mod_i - Mod_{aver}|)^2}$$

[d]: the Pearson's correlation (r)

163 **Table S5.** OH radical production reactions included in the model simulation

164

Source	Reactions
Primary Source	HONO photolysis
	$O^1D + H_2O$
	H_2O_2 photolysis
	VOCs + O_3
ROx propagation cycle	HO_2 + NO

165

166

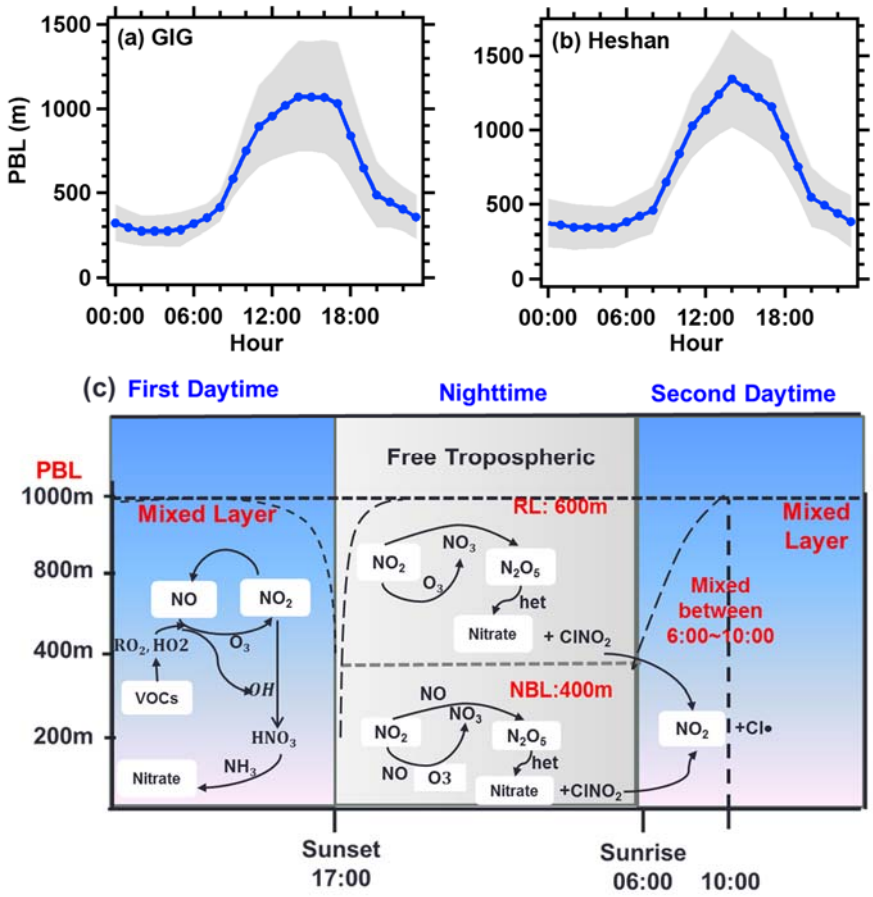

Figure S1. Diurnal variations of mean Planetary Boundary Layer (PBL) heights at (a) GIG site and (b) Heshan site, which were obtained from the NOAA Air Resource Laboratory website (https://ready.arl.noaa.gov/READYamet.php); (c) Schematic of PBL evolution and chemistry in the box model.

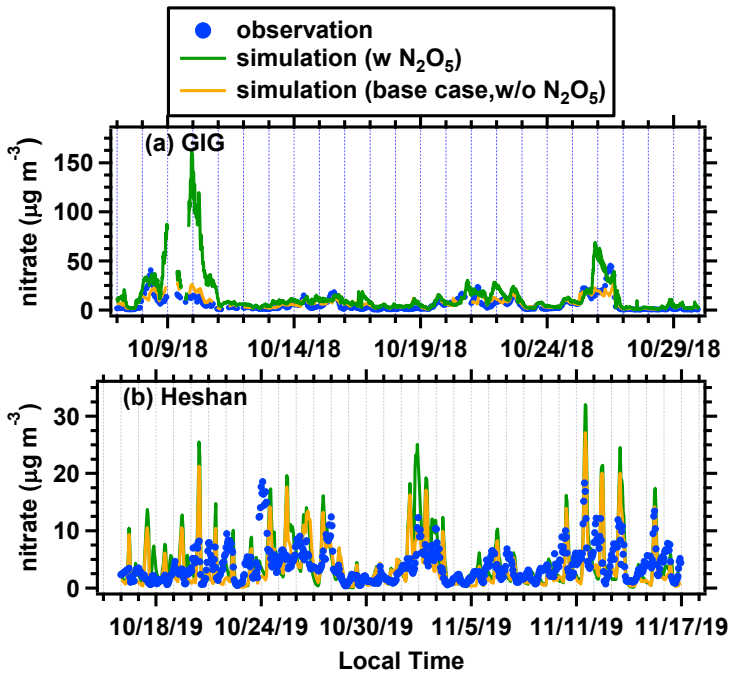

Figure S2. Comparison of the simulated and observed nitrate concentrations at (a) GIG site and (b) Heshan site. The orange lines represent simulated results of the base case without N_2O_5 constrained, and green lines represent the simulated results with N_2O_5 constrained.

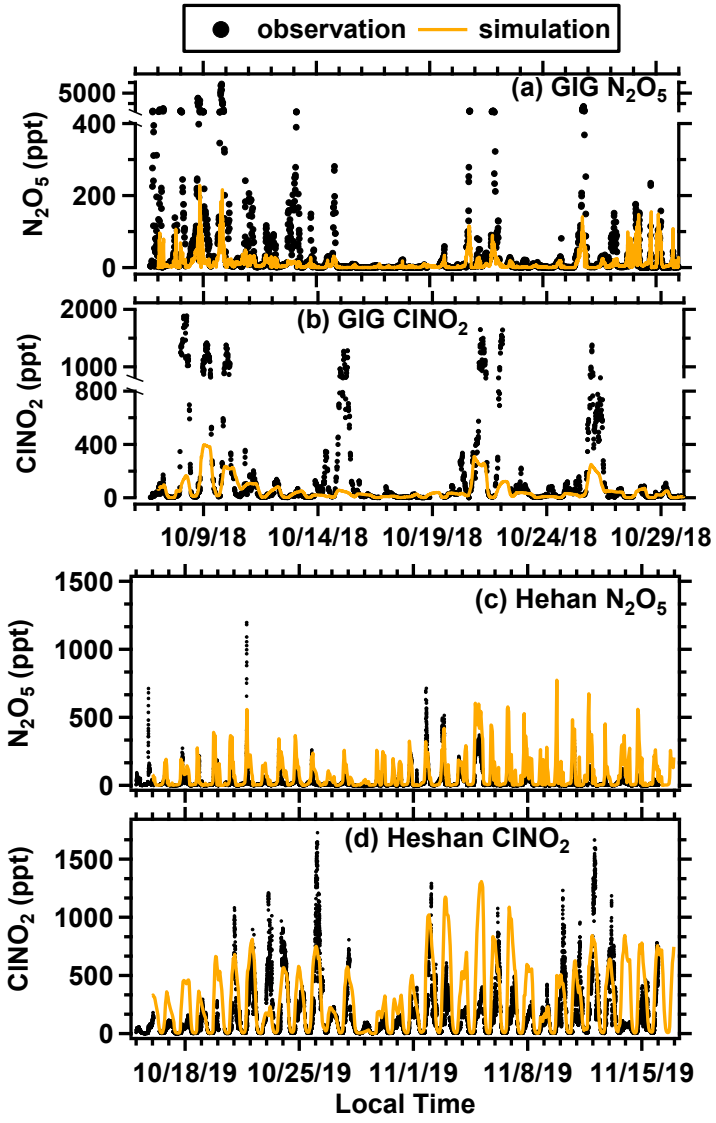

Figure S3. Comparison of the simulated and observed N_2O_5 and $ClNO_2$ concentrations at (a,b) GIG site and (c,d) Heshan site.

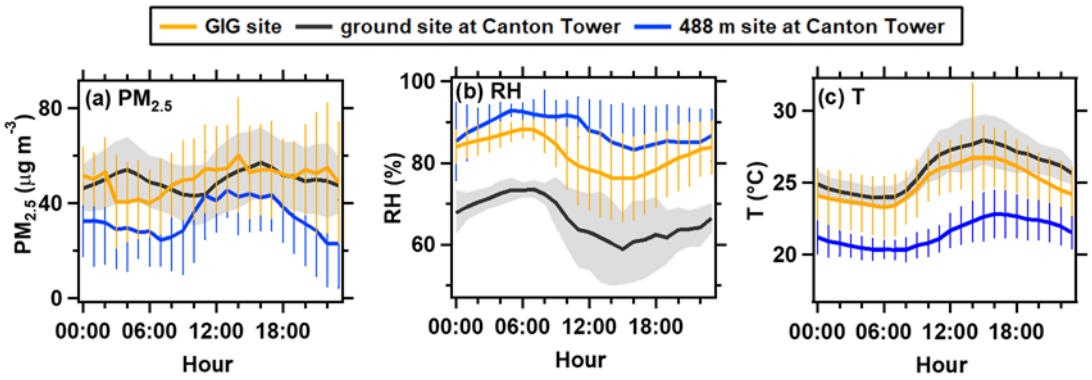

Figure S4. Diurnal variation of mean concentrations of (a) $PM_{2.5}$, (b) RH and (c) *T* at GIG, ground site and 488m site of Canton Tower. The orange lines represent the measurements at GIG site, and the blue and black lines represent the measurements at 488 m and ground site of Canton Tower, respectively. The orange and blue error bars represent the standard deviations of the mean concentrations at GIG site and 488m site of Canton Tower, and the grey areas show one standard deviation of the mean concentration at ground site of Canton Tower.

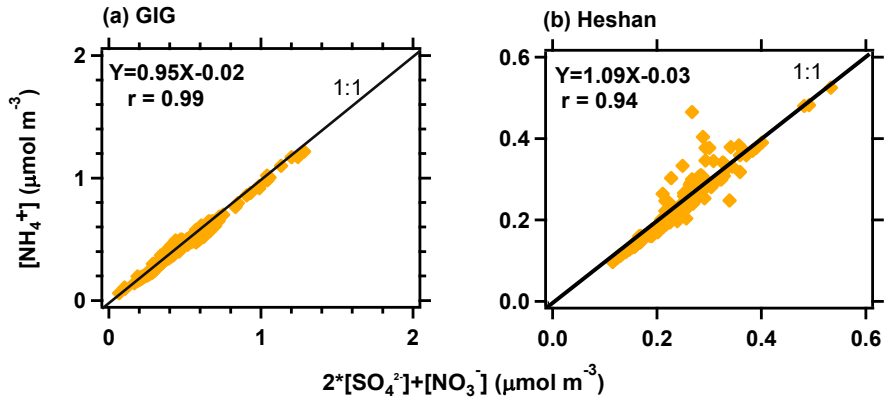

193

194 **Figure S5.** Scatter plot of [NH_4^+] molar concentration versus 2*[SO_4^{2-}] + [NO_3^-] at the

195 (a) GIG site and (b) Heshan site.

196

197

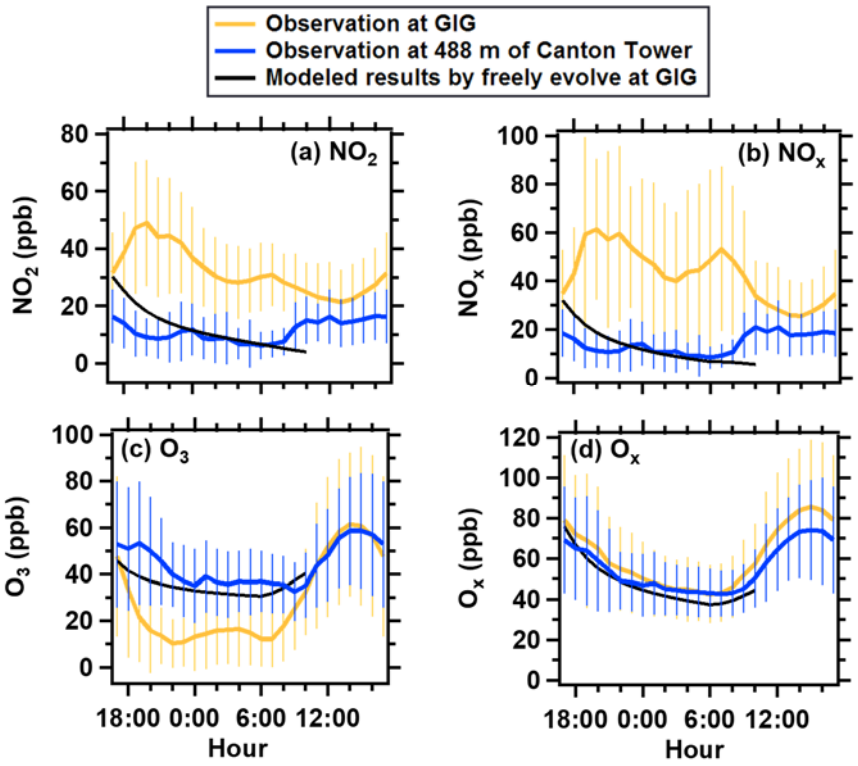

198

199 **Figure S6.** Time series of the simulated trace gases (NO_2, NO_x, O_3 and O_x) in the RL,
200 when the observations at 17:00 at GIG were setting as the initial inputs of the RL
201 simulation and all chemical species were freely evolved in the box model. The
202 observations at GIG and 488m site of Canton Tower are also shown for comparison.
203 The error bars represent the standard deviation of the observations.

204

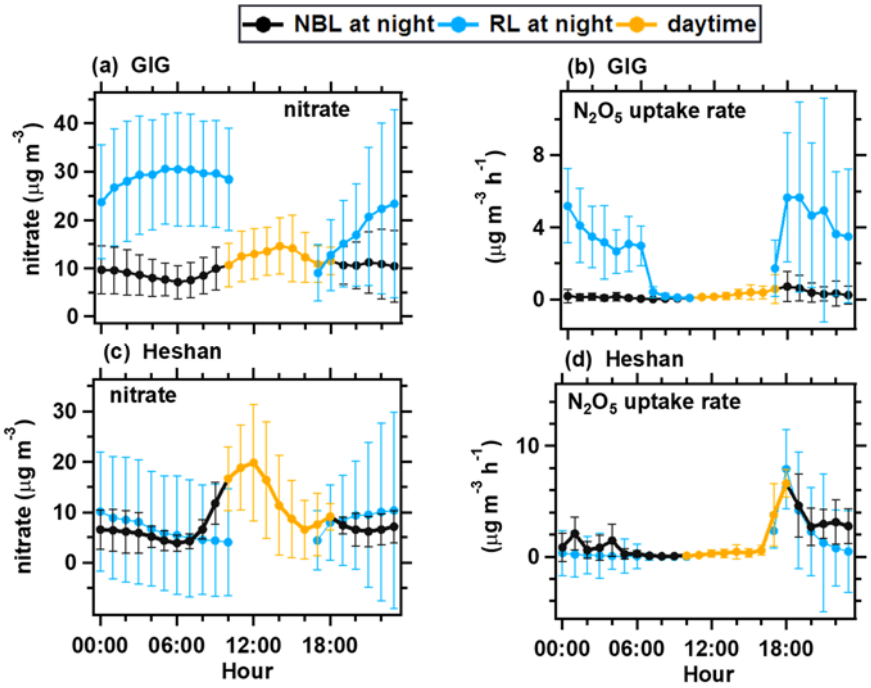

205

206 **Figure S7.** Comparison of the daily-averaged simulated nitrate and N_2O_5 uptake rate in

207 the NBL and RL at the (a, b) GIG site and (c, d) Heshan site**.** The error bars represent

208 the standard deviation of the average data.

209

210

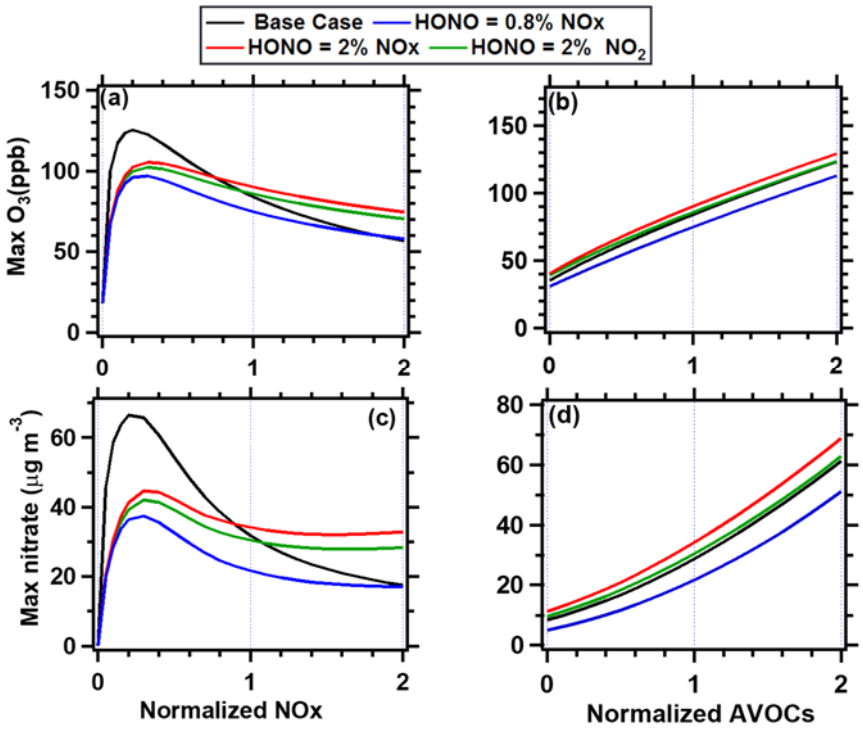

Figure S8. Sensitivity tests of HONO parameterization on the production of (a, b) ozone and (c, d) nitrate as a function of the normalized NOx and AVOCs relative to the base concentration at the GIG site.

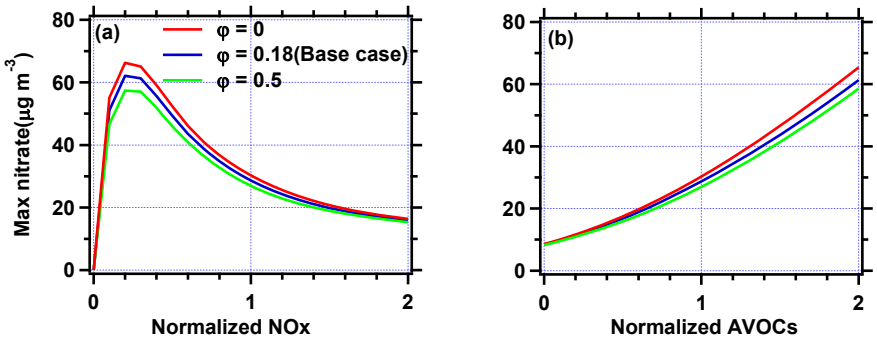

Figure S9. Sensitivity tests of the production yield of $ClNO_2$ (φ value) on maximum nitrate concentrations as a function of the normalized NOx and AVOCs relative to the base concentration at the GIG site.

Reference

Chen, X., Wang, H., Lu, K., Li, C., Zhai, T., Tan, Z., Ma, X., Yang, X., Liu, Y., Chen, S., Dong, H., Li, X., Wu, Z., Hu, M., Zeng, L., and Zhang, Y.: Field Determination of Nitrate Formation Pathway in Winter Beijing, Environmental Science & Technology, 10.1021/acs.est.0c00972, 2020.

Curci, G., Ferrero, L., Tuccella, P., Barnaba, F., Angelini, F., Bolzacchini, E., Carbone, C., Der Gon, H. A. C. D. V., Facchini, M. C., and Gobbi, G. P.: How much is particulate matter near the ground influenced by upper-level processes within and above the PBL? A summertime case study in Milan (Italy) evidences the distinctive role of nitrate, Atmospheric Chemistry and Physics, 15, 2629-2649, 2015.

Elshorbany, Y. F., Steil, B., Brühl, C., and Lelieveld, J.: Impact of HONO on global atmospheric chemistry calculated with an empirical parameterization in the EMAC model, Atmospheric Chemistry and Physics, 12, 9977-10000, 2012.

Kurtenbach, R., Becker, K. H., Gomes, J. A. G., Kleffmann, J., Lörzer, J. C., Spittler, M., Wiesen, P., Ackermann, R., Geyer, A., and Platt, U.: Investigations of emissions and heterogeneous formation of HONO in a road traffic tunnel, Atmospheric Environment, 35, 3385-3394, https://doi.org/10.1016/S1352-2310(01)00138-8, 2001.

Lammel, G., and Cape, J. N.: Nitrous acid and nitrite in the atmosphere, Chemical Society Reviews, 25, 361-369, 10.1039/CS9962500361, 1996.

Lin, Y. C., Zhang, Y. L., Fan, M. Y., and Bao, M.: Heterogeneous formation of particulate nitrate under ammonium-rich regimes during the high-PM2.5 events in Nanjing, China, Atmos. Chem. Phys., 20, 3999-4011, 10.5194/acp-20-3999-2020, 2020.

McDuffie, E. E., Fibiger, D. L., Dubé, W. P., Lopez-Hilfiker, F., Lee, B. H., Thornton, J. A., Shah, V., Jaeglé, L., Guo, H., Weber, R. J., Michael Reeves, J., Weinheimer, A. J., Schroder, J. C., Campuzano-Jost, P., Jimenez, J. L., Dibb, J. E., Veres, P., Ebben, C., Sparks, T. L., Wooldridge, P. J., Cohen, R. C., Hornbrook, R. S., Apel, E. C., Campos, T., Hall, S. R., Ullmann, K., and Brown, S. S.: Heterogeneous N2O5 Uptake During Winter: Aircraft Measurements During the 2015 WINTER Campaign and Critical Evaluation of Current Parameterizations, Journal of Geophysical Research: Atmospheres, 123, 4345-4372, 10.1002/2018JD028336, 2018.

Mozurkewich, M., and Calvert, J. G.: Reaction probability of N2O5 on aqueous aerosols, Journal of Geophysical Research: Atmospheres, 93, 15889-15896, 10.1029/JD093iD12p15889, 1988.

Riedel, T. P., Wolfe, G. M., Danas, K. T., Gilman, J. B., Kuster, W. C., Bon, D. M., Vlasenko, A., Li, S. M., Williams, E. J., Lerner, B. M., Veres, P. R., Roberts, J. M., Holloway, J. S., Lefer, B., Brown, S. S., and Thornton, J. A.: An MCM modeling study of nitryl chloride (ClNO₂) impacts on oxidation, ozone production and nitrogen oxide partitioning in polluted continental outflow, Atmos. Chem. Phys., 14, 3789-3800, 10.5194/acp-14-3789-2014, 2014.

Tan, Z., Lu, K., Jiang, M., Su, R., Wang, H., Lou, S., Fu, Q., Zhai, C., Tan, Q., Yue, D., Chen, D., Wang, Z., Xie, S., Zeng, L., and Zhang, Y.: Daytime atmospheric oxidation capacity in four Chinese megacities during the photochemically polluted season: a case study based on box model simulation, Atmos. Chem. Phys., 19, 3493-3513, 10.5194/acp-19-3493-2019, 2019.

Wang, H., Lu, K., Chen, X., Zhu, Q., Chen, Q., Guo, S., Jiang, M., Li, X., Shang, D., Tan, Z., Wu, Y., Wu, Z., Zou, Q., Zheng, Y., Zeng, L., Zhu, T., Hu, M., and Zhang, Y.: High N2O5 Concentrations Observed in Urban Beijing: Implications of a Large Nitrate Formation Pathway, Environmental Science & Technology Letters, 4, 416-420, 10.1021/acs.estlett.7b00341, 2017.

Womack, C. C., McDuffie, E. E., Edwards, P. M., Bares, R., de Gouw, J. A., Docherty, K. S., Dube, W. P., Fibiger, D. L., Franchin, A., Gilman, J. B., Goldberger, L., Lee, B. H., Lin, J. C., Long, R., Middlebrook, A. M., Millet, D. B., Moravek, A., Murphy, J. G., Quinn, P. K., Riedel, T. P., Roberts, J. M., Thornton, J. A., Valin, L. C., Veres, P. R., Whitehill, A. R., Wild, R. J., Warneke, C., Yuan, B., Baasandorj, M., and Brown, S. S.: An odd oxygen framework for wintertime ammonium nitrate aerosol pollution in urban areas: NOx and VOC control as mitigation strategies, Geophysical Research Letters, 0, 10.1029/2019gl082028, 2019.

Yu, C., Wang, Z., Xia, M., Fu, X., Wang, W., Tham, Y. J., Chen, T., Zheng, P., Li, H., Shan, Y., Wang, X., Xue, L., Zhou, Y., Yue, D., Ou, Y., Gao, J., Lu, K., Brown, S. S., Zhang, Y., and Wang, T.: Heterogeneous N2O5 reactions on atmospheric aerosols at four Chinese sites: improving model representation of uptake parameters, Atmos. Chem. Phys., 20, 4367-4378, 10.5194/acp-20-4367-2020, 2020.

Yun, H., Wang, W., Wang, T., Xia, M., Yu, C., Wang, Z., Poon, S. C. N., Yue, D., and Zhou, Y.: Nitrate formation from heterogeneous uptake of dinitrogen pentoxide during a severe winter haze in southern China, Atmos. Chem. Phys., 18, 17515-17527, 10.5194/acp-18-17515-2018, 2018.

Zhang, L., Brook, J. R., and Vet, R.: A revised parameterization for gaseous dry deposition in air-quality models, Atmos. Chem. Phys., 3, 2067-2082, 10.5194/acp-3-2067-2003, 2003.